Development and Propagation of Equatorial Waves

*Xiaofan Li*① and *Han-Ru Cho*

Department of Physics, University of Toronto, Toronto, Ontario, Canada, M5S 1A7

Received November 18, 1996; revised January 13, 1997

ABSTRACT

Development and propagation of equatorial waves are investigated with the model which includes convection-wave convergence feedback and convection-frictional convergence feedback. Two experiments with an initial Kelvin wave (Exp. K) and with an initial Rossby wave (Exp. R) are carried out. The equatorial waves in Exp. R grow much faster than those in Exp. K. The equatorial waves in both experiments follow zonal (eastward / westward) and meridional (poleward) propagation.

The equatorial waves can be partitioned into two meridional modes using Parabolic Cylinder Function. An equator mode denotes a wave component with a positive precipitation center at the equator and an off-equator mode represents a wave component with positive precipitation centers off the equator. The equator mode dominates in Exp. K whereeas the off-equator mode dominates in Exp. R. The rapid wave growth in Exp. R is interpreted by analyzing the eddy available potential energy (EAPE) generation. Stronger off-equator mode in Exp. R obtains more EAPE through convection-frictional convergence feedback which results in more rapid wave growth.

The relative vorticity tendency is determined by interactions between Earth's vorticity and lower-troposphere convergence (divergence effect) and between the meridional gradient and lower-troposphere circulation (beta effect). The eastward and poleward propagation of equatorial waves is a result of the divergence effect, and the westward movement is caused by the beta effect.

Key words: Equatorial waves, Development, Propagation, Eddy available potential energy, Vorticity tendency

I. INTRODUCTION

Madden and Julian (1971, 1972) first noticed an eastward propagation of large scale cells with a period of 40-50 days over the equatorial troposphere. Such an oscillation is later referred to as Madden-Julian Oscillation (MJO). Since its discovery, three major theories have been proposed to explain the MJO as the eastward propagating equatorial Kelvin waves. Lau and Peng (1987), and Change and Lim (1988) suggested that the slow eastward propagation of intraseasonal oscillation results from an interaction of convection through the wave-CISK mechanism (Hayashi, 1970; Lindzen, 1974). Emanuel (1987) and Neelin et al. (1987) proposed that in the presence of a uniform easterly basic flow, the interaction between anomalous evaporation and surface wind could cause the asymmetric heating along the equator, inducing a slow eastward wave propagation. Wang (1988) and Wang and Li (1994) posed another mechanism considering the interaction between waves and boundary-layer convergence. Such an interaction favors the growth of planetary-scale waves.

Although equatorial Kelvin and Rossby waves are the twin formed from the symmetric heating source centered along the equator, their dynamic structures are very different (e. g.,

①Corresponding author address: Dr. Xiaofan Li, Applied Research Corporation, NASA / Goddard Space Flight Center, Code 913, Greenbelt, MD 20771, USA.

Gill, 1980). Furthermore, the equatorial Kelvin waves may account for the eastward-propagating intraseasonal oscillation, whereas the equatorial Rossby waves may explain the twin cyclogenesis associated with the westerly wind burst along the equator (e. g., Kuma, 1994). Previous studies have been focused on the equatorial Kelvin waves. Thus, there is a necessity to investigate the equatorial Rossby waves in comparison with the equatorial Kelvin waves. The goal of this study is to examine the structures, development, and propagation of the equatorial waves under the mechanisms of convection-wave convergence feedback and convection-frictional convergence feedback. Development of the equatorial waves with other mechanisms will be reported in a separate paper. Mainly, we answer the following questions: What are differences of dynamic characteristics among a Kelvin wave and a long Rossby wave and their induced waves? What are energy sources responsible for development of the equatorial waves? what processes determine the wave propagation? We will describe the model and experiments in the next section briefly. Then we examine the structures of equatorial waves partitioning the meridional mode with Parabolic Cylinder Function in the Section 3. We derive a set of energetics equations and discuss energy budgets in Section 4, and construct an equation of relative vorticity tendency and discuss the causes of propagation in Section 5. We will summarize the main finding in Section 6.

II. MODEL AND EXPERIMENTS

The model used in this study was originally developed by Wang and Li (1993, 1994). The detailed derivation of the model can be found in their papers. Here we only briefly describe the model. The model consists of a two-layer free troposphere and a well-mixed boundary layer. Under the assumption that the column integral of divergence in the troposphere vanishes, the model contains only two vertical modes: the free-troposphere baroclinic mode, and the boundary-layer induced barotropic mode. The model physics includes convection-wave convergence feedback and convection-frictional convergence feedback. The governing equations on an equatorial beta-plane are:

$$\frac{\partial u}{\partial t} = \beta y v - \frac{\partial \varphi}{\partial x} + r\nabla^2 u \ , \tag{2.1a}$$

$$\frac{\partial v}{\partial t} = -\beta y u - \frac{\partial \varphi}{\partial y} + r\nabla^2 v \ , \tag{2.1b}$$

$$C_0^{-2}\frac{\partial \varphi}{\partial t} = -(1 - HI)\nabla \cdot \vec{V} + d(HB - 1)\nabla \cdot \vec{V}_B \ , \tag{2.1c}$$

$$\beta y v_B - \frac{\partial \varphi}{\partial x} - E u_B = 0 \ , \tag{2.1d}$$

$$-\beta y u_B - \frac{\partial \varphi}{\partial y} - 2E v_B = 0 \ . \tag{2.1e}$$

Here $\vec{V}(u,v)$ and $\vec{V}_B(u_B,v_B)$ are the lower-troposphere and boundary-layer winds, respectively; φ is the lower-troposphere geopotential perturbation; β is the meridional gradient of Earth's vorticity; r is a horizontal momentum diffusion coefficient, C_0

denotes dry gravity wave speed of the free-troposphere baroclinic mode; $d=\frac{(P_s-P_e)}{\Delta P}$ is nondimensional depth of the boundary layer, ΔP is one-half pressure depth of the free troposphere, P_s and P_e are the pressures of surface and the top of the boundary layer; E is an Ekman number in the boundary layer; The nondimensional parameters $I=\frac{q_3}{q_c}$ and $B=\frac{q_e}{q_c}$ are the heating coefficient due to wave convergence in the free lower troposphere and the heating coefficient due to frictional convergence in the boundary layer respectively, and both are functions of sea surface temperature (Wang and Li, 1994), where $q_c=\frac{2c_p p_2 C_0^2}{bR\Delta pL_c}$, and R, L_c, c_p, b are gas constant for dry air, latent heat of condensation, and specific heat at constant pressure, a coefficient of condensation efficiency measuring the fraction of total moisture convergence that condenses out as precipitation respectively; q_e and q_3 are, respectively, vertical mean specific humidity in the boundary layer and in the lower tropospheric layer; a conditional heating scheme (Wang and Li, 1993) is adopted which allows latent heat release only with positive precipitation, and thus $H=H(M)$ is a Heaviside step function of M, where M is defined as

$$M=\frac{b[-\omega_2 q_3-\omega_e(q_e-q_3)]}{g}, \tag{2.2}$$

and the precipitation rate $P_r=HM$ (Wang, 1988). In Eq.(2.2), ω_e and ω_2 represent, respectively, vertical pressure velocities at the top of the boundary layer (p_e) and the midtrposphere (p_2), and g is the gravitational acceleration rate. The basic parameters chosen in this study are identical to those used by Wang and Li (1994) (see Table 1 of their paper). In Eqs. (2.1d) and (2.1e), the local change of boundary-layer flows is not included, and the meridional friction coefficient is twice larger than its zonal coefficient (Wang and Li, 1994).

For convenience, we scale horizontal velocity $\vec{V}$ and $\vec{V}_B$ by $(1-I)C_0$, geopotential φ by $[(1-I)C_0]^2$, time t by $(2\beta(1-I)C_0)^{-\frac{1}{2}}$, horizontal coordinates x,y by $\left[\frac{(1-I)C_0}{2\beta}\right]^{\frac{1}{2}}$. The nondimensional governing equations are derived from (2.1):

$$\frac{\partial u}{\partial t}=\frac{1}{2}yv-\frac{\partial\varphi}{\partial x}+r^*\nabla^2 u, \tag{2.3a}$$

$$\frac{\partial v}{\partial t}=-\frac{1}{2}yu-\frac{\partial\varphi}{\partial y}+r^*\nabla^2 v, \tag{2.3b}$$

$$\frac{\partial\varphi}{\partial t}=-\frac{(1-HI)}{(1-I)}\nabla\cdot\vec{V}+\frac{d(HB-1)}{(1-I)}\nabla\cdot\vec{V}_B, \tag{2.3c}$$

$$\frac{1}{2}yv_B-\frac{\partial\varphi}{\partial x}-E^* u_B=0, \tag{2.3d}$$

$$-\frac{1}{2}yu_B-\frac{\partial\varphi}{\partial y}-2E^* v_B=0, \tag{2.3e}$$

where $r^* = r\left[\frac{C_0^3(1-I)^3}{2\beta}\right]^{-\frac{1}{2}}$, and $E^* = E[2\beta C_0(1-I)]^{-\frac{1}{2}}$.

Wang and Li (1994) carried out an experiment with an initial Kelvin wave to examine the MJO revealed by the eastward propagating equatorial Kelvin waves. In their experiment, the equatorial Rossby waves were only induced during the integration. To investigate the equatorial Rossby waves, we performed an experiment with an initial long Rossby wave (Exp. R) as well as an experiment with an initial Kelvin wave (Exp. K) for comparison. Exp. K is the same as that done by Wang and Li (1994). The initial fields for both experiments are constructed from the steady solutions of Gill's model (1980), i.e., his Eqs. (4.2) and (4.3) for Exp. K and Eqs. (4.7) and (4.8) for Exp. R. The zonal scales of the initial equatorial waves are 4000 km. The model domain extends from 50°S to 50°N with the mesh 5° longitude by 2° latitude. The model is integrated for 20 days. The uniform sea surface temperature is 29°C, and the top of the boundary layer is at 900 hPa (P_e). Sensitivity tests show that the growth rates of both equatorial Kelvin and Rossby waves increase with increasing sea surface temperature and increasing thickness of the boundary layer which decreases P_e (also see Wang and Li, 1994).

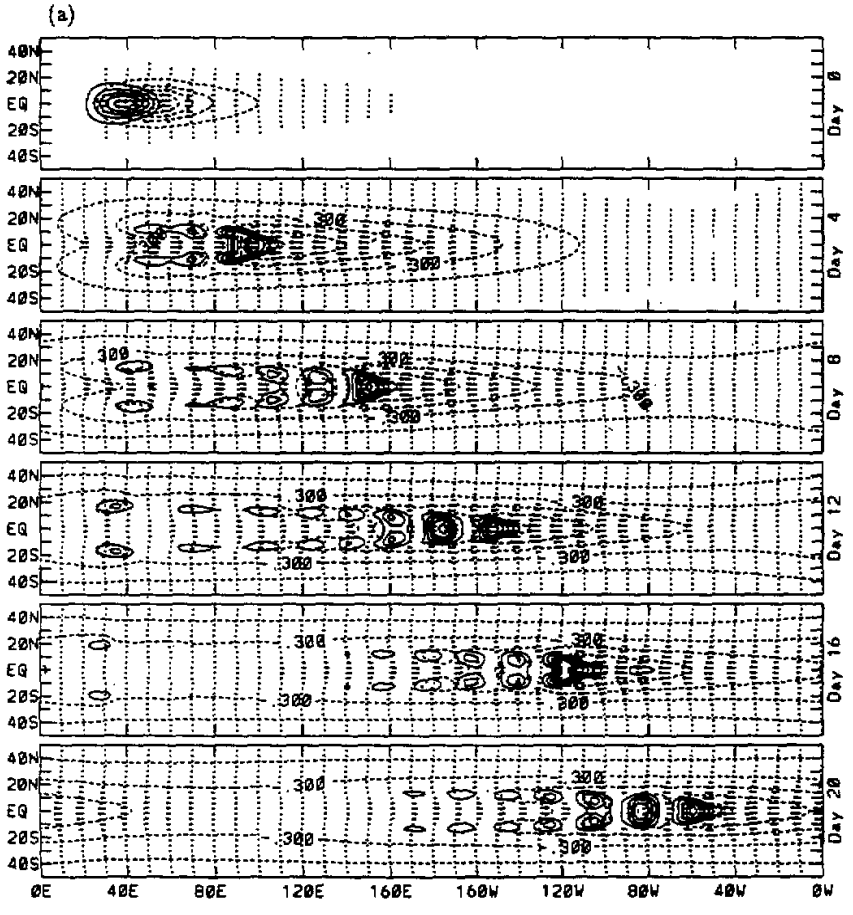

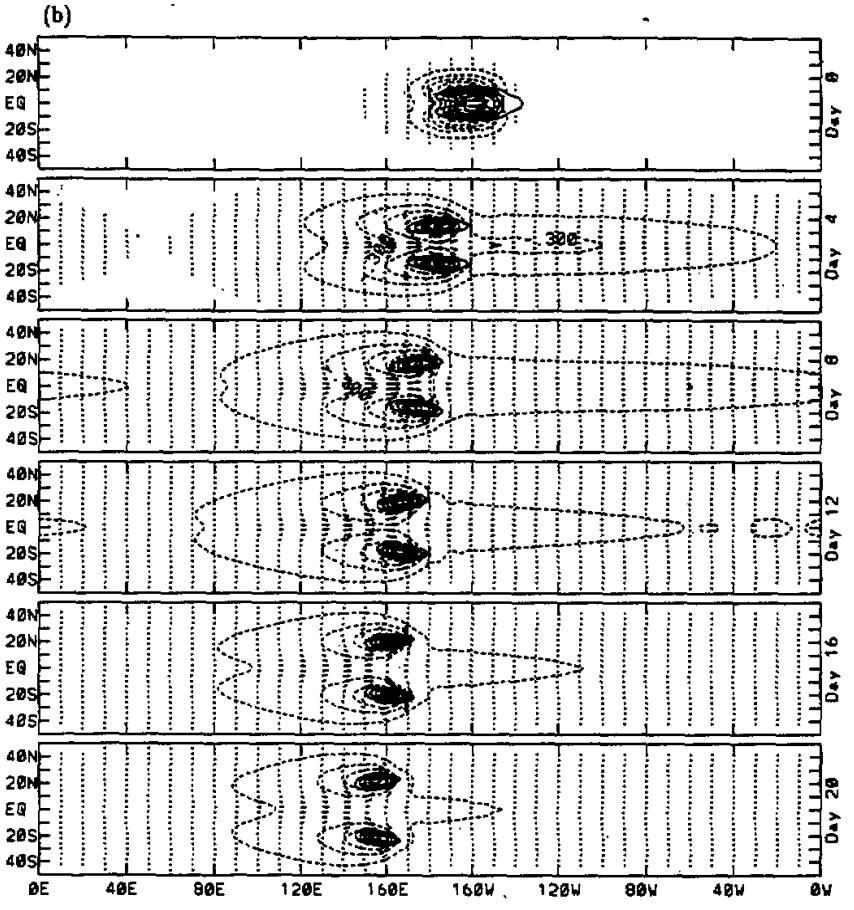

Fig. 1. Precipitation rate (solid-line contours), Lower-troposphere geopotential perturbation (dashed-line contours), and wind (arrow) within 20 days at an interval of 4 days in (a) Exp. K and (b) Exp. R. All three fields are normalized by their respective maxima at each panel. The contour starts from 0.1 at an interval of 0.2.

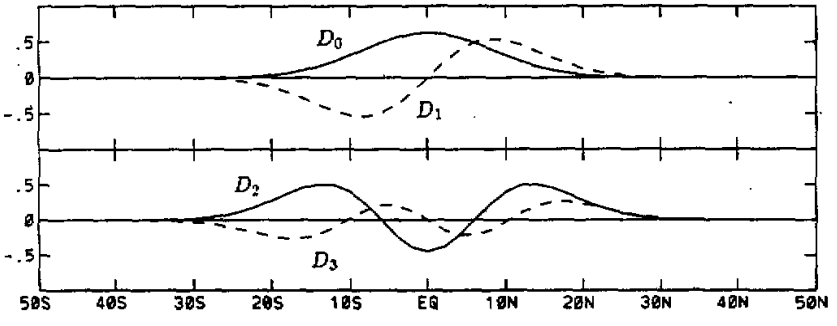

Fig. 2. Latitudinal variations of parabolic cylinder functions D_0, D_1, D_2, and D_3.

Although the zonal scales of initial equatorial waves in Exps. K and R are the same, the scale of the waves in Exp. K grows whereas that in Exp. R remains the same as their initial zonal scale (Fig. 1). As a result, the waves have much larger zonal scales in Exp. K than in Exp. R. The exponential growth rate of the waves estimated from their precipitation rate in Exp. R (0.31 day^{-1}) is about the twice as large as that in Exp. K (0.17 day^{-1}). The waves whose precipitation rates reach maxima at the equator in Exp. K propagate eastward persistently. The initial Kelvin wave also induces the waves whose precipitation rates reach maxima off the equator. Because of the presence of the boundary layer, Rossby waves are generated at the trailing edge of the Kelvin waves. The leading Kelvin wave propagates rapidly eastward, while the trailing Rossby waves propagate slowly westward and poleward. The Rossby waves eventually die offf some distance away from the leading Kelvin wave (Fig. 1a). In Exp. R, the centers of precipitation were originally located very close to the equator, then move quickly away from the equator during the period of adjustment, followed by slow westward and

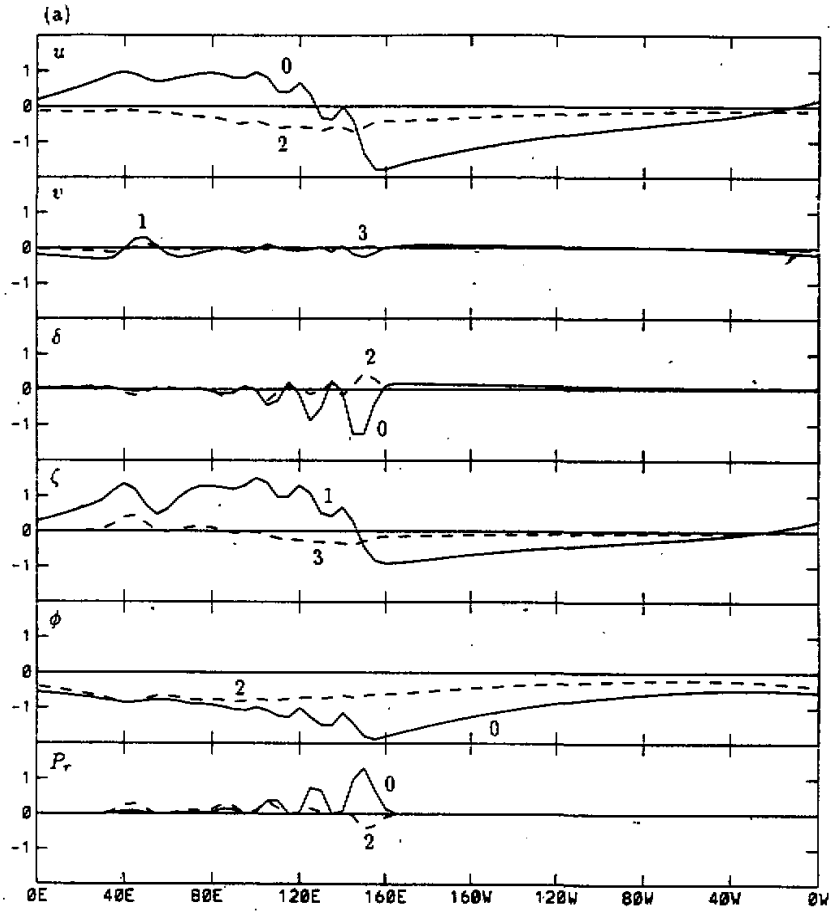

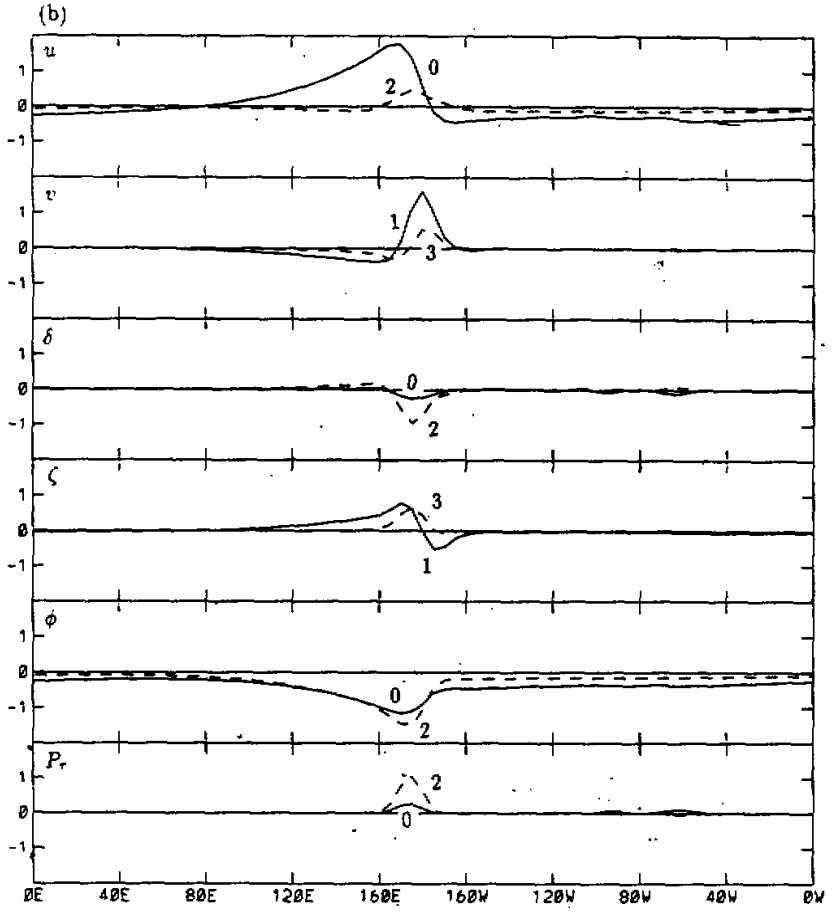

Fig. 3. Longitudinal distributions of meridional modes for wind (u,v), divergence (δ), vorticity (ζ), geopotential (φ) in the lower troposphere and precipitation rate (P_r) at day 8 in (a) Exp. K and (b) Exp. R.

poleward propagation (Fig. 1b). These experiments suggest that the growth rates as well as the waves forms that eventually develop will depend on the initial structure of the disturbance. The wave structures are thus analyzed in the next section.

III. PARTITIONING OF MERIDIONAL MODES

Gill (1980) derived the analytic solutions for the Kelvin and the long Rossby waves forced by symmetric heating about the equator using the Parabolic Cylinder Function (PCF). In kelvin waves the meridional structures of zonal wind and the geopotential are dominated by the order–0 mode of the PCF's while the meridional velocity is zero. Rossby waves are characterized by all modes $n \geqslant 0$ in the zonal velocity, the geopotential, as well as the meridional velocity. To analyze the wave structures, the meridional structures of the wave fields are decomposed into PCF's. A variable F can be expressed as

$$F = \sum_{i=0}^{\infty} F_i(x,y,t) \ , \tag{3.1}$$

where $F_i = f_i(x,t)D_i(y)$, and $D_i(y)$ is order-i PCF; the first four PCF's (Fig. 2) are:

$$(D_0,D_1,D_2,D_3) = [(2\pi)^{-\frac{1}{4}},(2\pi)^{-\frac{1}{4}}y,(8\pi)^{\frac{-1}{4}}(y^2-1),(882\pi)^{\frac{-1}{4}}(y^3-y)]e^{-\frac{1}{4}y^2} \ , \tag{3.1a}$$

and

$$f_i = \int_{-\infty}^{+\infty} F_i D_i dy \ , \tag{3.1b}$$

Since the meridional modes are similar during the integrations, we show the meridional modes at day 8 for both Exps. K and R. In both Experiments, even meridional modes

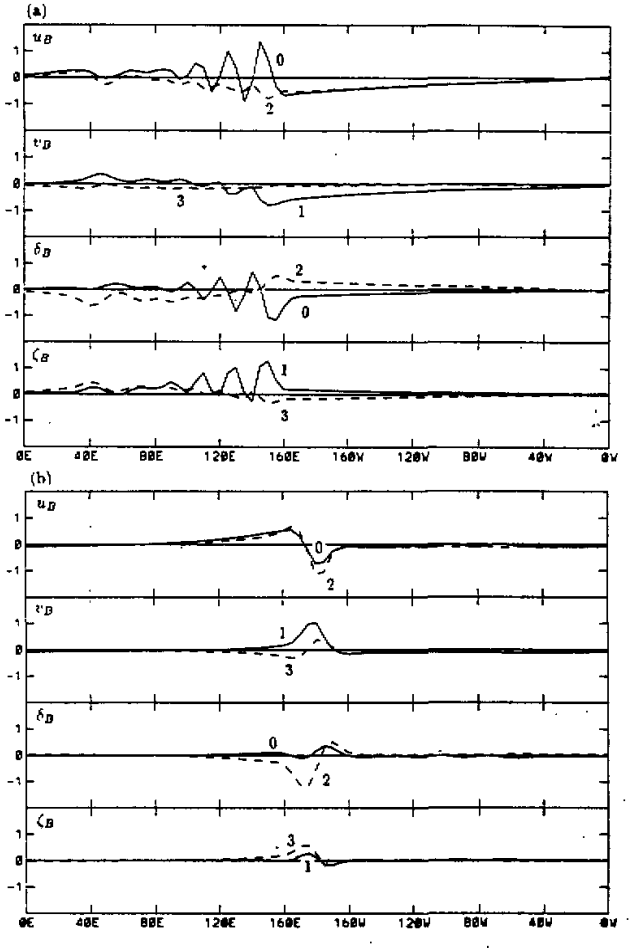

Fig. 4. Longitudinal distributions of meridional modes for wind (u_B,v_B), divergence (δ_B), and vorticity (ζ_B) in the boundary layer at day 8 in (a) Exp. K and (b) Exp. R.

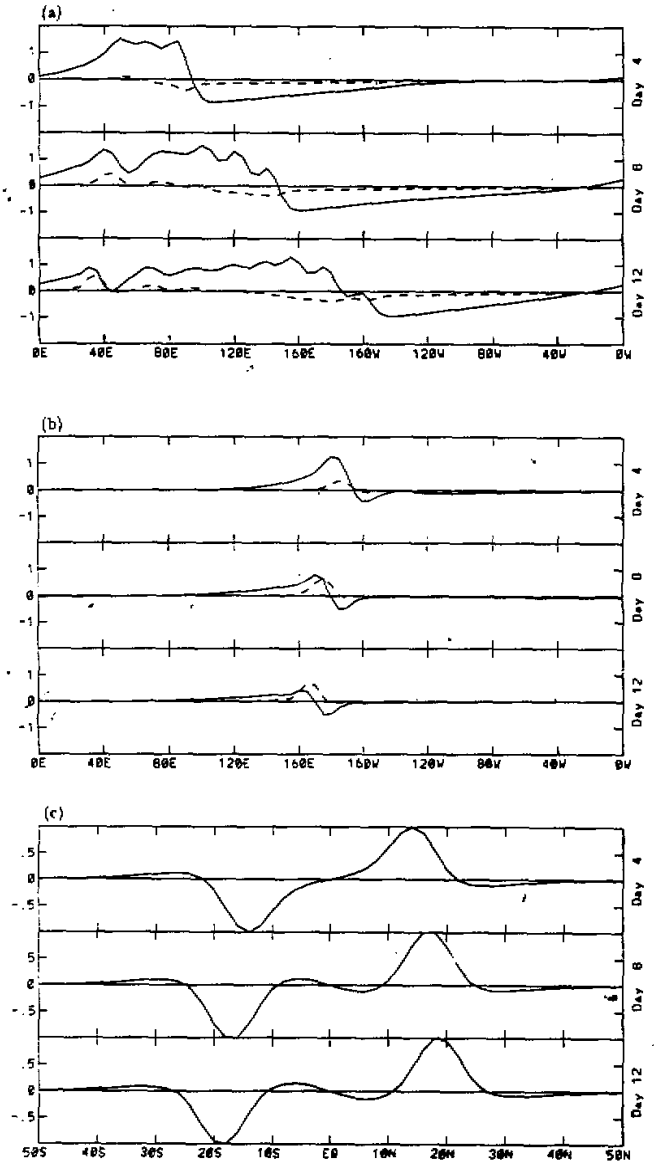

Fig. 5. The evolution of longitudinal distributions of ζ_1 (solid lines) and ζ_3 (dashed lines) in (a) Exp. K and (b) Exp. R, and (c) latitudinal distributions of ζ along the longitude where it reaches maximum in Exp. R.

(modes 0 and 2) dominate in zonal wind, divergence both in the lower tropsphere (Fig. 3) and in the boundary layer (Fig. 4), geopotential and precipitation rate (Fig. 3), whereas odd meridional modes (modes 1 and 3) dominate in meridional wind, relative vorticity both in the lower troposphere (Fig. 3) and in the boundary layer (Fig. 4).

In the lower troposphere (Fig. 3), amplitude of u_0 is larger than that of u_2. u_0 is negative to the east of 140°E and positive to the west in Exp. K, indicating easterly wind to the east and westerly wind to the west at the equator. The modes for the meridional wind are much stronger in Exp. R than those in Exp. K. In Exp. R, v_1 has larger amplitude than that of v_3, and is positive with its maximum between maximum and minimum of u_0. Comparing the meridional structures of u and v, we can conclude that in Exp. K, the u_0 mode has a very large component of Kelvin wave and a minor component of order-1 Rossby wave (corresponding to v_1, and also the non-negligible u_2). In Exp. R, u_0 and v_1 are due mostly to an order-1 Rossby wave. Convergence is mainly contributed by δ_0 and δ_2, respectively, in Exps. K and R. ζ_1 is a major contributor to relative vorticity in Exp. K whereas ζ_1 and ζ_3 are equally important in Exp. R. Note that the zonal scale of ζ_3 is smaller than that of ζ_1 in Exp. R. φ_0 has larger amplitude than φ_2 in Exp. K whereas φ_0 and φ_2 have similar amplitude in Exp. R. The meridional modes of precipitation rate (P_r) resemble those of δ and δ_B.

In the boundary layer (Fig. 4), amplitude of u_{B0} is larger than u_{B2} in Exp. K wheresas amplitudes of u_{B0} and u_{B2} are about the same in Exp. R. Both experiments show that v_{B1} has larger amplitude than v_{B3}. Convergence is dominated by δ_{B0} in Exp. K and by δ_{B2} in Exp. R, whereas relative vorticity is dominated by ζ_{B1} in Exp. K and by ζ_{B3} in Exp. R.

The evolution of the meridional modes indicates that in Exp. K (Fig. 5a) maxima of ζ_1 associated with the Kelvin waves move eastward while maximum of ζ_1 of the Rossby waves moves westward. In Exp. R, both ζ_1 and ζ_3 of Rossby waves propagate westward (Fig. 5b) as well as poleward (Fig. 5c).

IV. DEVELOPMENT OF EQUATORIAL WAVES

In this section the energetics of the equatorial waves will be analyzed. It is convenient to define equator mode and off-equator mode as order-0 PCF mode and sum of PCF modes $n \geq 0$ respectively. The equator mode represents the wave structure with a positive precipitation center at the equator whereas the off-equator mode denotes the wave structure with positive precipitation centers off the equator. A field F (u,v,φ,u_B ,or v_B) can be thus decomposed in the meridional direction by the equator mode (F_0) and off-equator mode (F_1):

$$F = F_0 + F_1 \quad . \tag{4.1}$$

Note F_1 in this section is different from that in the last section.

The dimensionless kinetic energy (KE) equations can be derived by multiplying (2.3a) by u_i and (2.3b) by v_i, respectively, and integrating the equations over the model domain,

$$\frac{\partial K_i}{\partial t} = \sum_{j=0}^{1} [(K_i, K_j) + (P_j, K_i)] + DK_i \quad , \tag{4.2}$$

where subscript "i" is 0 for equator mode or 1 for off-equator mode.

The dimensionless eddy available potential energy (EAPE) equations can be derived by multiplying (2.3c) by φ_i and integrating the equations over the model domain,

$$\frac{\partial P_i}{\partial t} = \sum_{j=0}^{1} [-(P_i,K_j) + GP_i + GPB_i] \ . \tag{4.3}$$

In (4.2) and (4.3),

$$K_i = < \frac{u_i^2 + v_i^2}{2} > \tag{4.4a}$$

and

$$P_i = < \frac{\varphi_i^2}{2} > \tag{4.4b}$$

are dimensionless KE and EAPE for each mode ($i = 0,1$), and

$$(K_i,K_j) = \frac{1}{2} < y(v_i u_j - u_i v_j) > \ . \tag{4.4c}$$

and

$$(P_i,K_j) = < \varphi_i \left(\frac{\partial u_j}{\partial x} + \frac{\partial v_j}{\partial y} \right) > \tag{4.4d}$$

are dimensionless energy conversion terms, in which (A,B) means energy conversion from A to B and $(A,B) = -(B,A)$, and

$$GP_i = < -\frac{1-H}{1-I} I\varphi_i \nabla \cdot \vec{V} > \tag{4.4e}$$

and

$$GPB_i = < -d\frac{1-HB}{1-I} \varphi_i \nabla \cdot \vec{V}_B > \tag{4.4f}$$

are dimensionless generation terms of EAPE by the convection–wave convergence feedback and by the convection–frictional convergence feedback, respectively, and

$$DK_i = r^* < (u_i \nabla^2 u + v_i \nabla^2 v) > \tag{4.4g}$$

is the KE dissipation term.

As can be seen in Fig. 6, KE is much smaller than EAPE. P_0 is larger than P_1 in Exp. K (Fig. 6a) whereas P_0 is smaller than P_1 in Exp. R (Fig. 6b). This is consistent with the fact that equator mode dominates in Exp. K and off-equator mode dominates in Exp. R. The EAPE in Exp. K increases from 79.75 at day 8 to 2181.1 at day 16, whereas the EAPE in Exp. R increases from 57.6 at day 8 to 3424.7 at day 16. This indicates that the EAPE increases much faster in Exp. R than in Exp. K, consistent with the wave growth rates discussed earlier because the generation rates of EAPE due to GP in both experiments are about the same (5.81 in Exp. K vs 6.14 in Exp. R), and the generation rates of P_0 due to GPB are similar (3.37 in Exp. K vs 3.66 in Exp. R). The difference of generation rates of the EAPE between both experiments is mainly due to the difference of GPB_1. It is the large generation rate of GPB_1 in Exp. R that causes rapid growth of the EAPE compared to the EAPE in Exp. K. Why is GPB_1 much larger in Exp. R than in Exp. K? First, the off-equator mode of the geotential is much stronger in Exp. R than in Exp. K. Second, the values in the angle bracket of Eq. (4.4f) associated with the off-equator mode are positive over the entire model domain in Exp. R, whereas they are negative and positive in Exp. K. Thus, their integration GPB_1 in Exp. R is much larger than that in Exp. K.

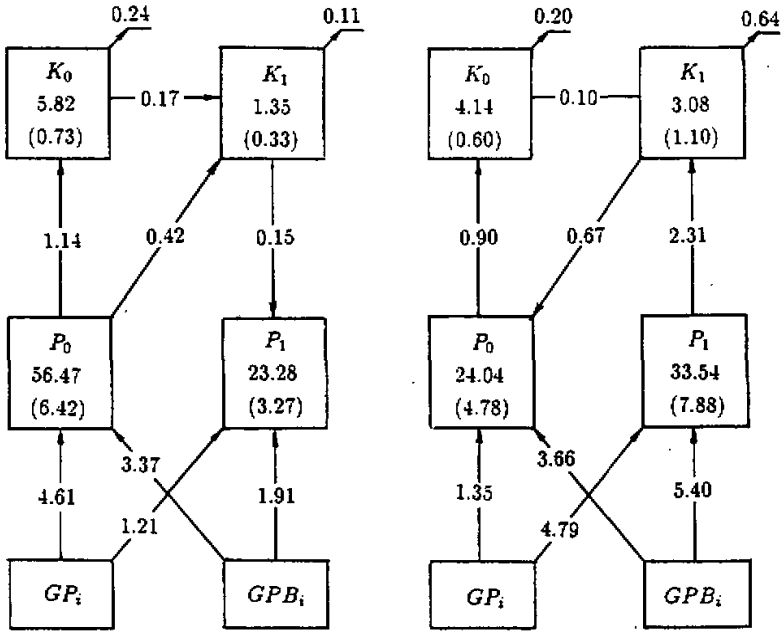

Fig. 6. Energy budgets at day 8 in (a) Exp. K and (b) Exp. R. The values in boxes denote the energy whereas the values in bracket present the energy generation rates. The values at the upper right of the kinetic energy boxes are the dissipation rates. The other values denote the energy conversions and energy generations *GP* and *GPB*. All values are nondimensional. the arrows indicate direction of energy transfer.

V. PROPAGATION OF EQUATIORIAL WAVES

Li and Wang (1994) pointed out that analyzing the vorticity tendency is an effective way to determine the cause of beta-gyre movement in their beta-drift theory. Thus an equation of vorticity tendency is derived to determine the dominant dynamic processes which control the equatorial wave propagation. The nondimensional equation of vorticity tendency can be expressed as

$$\frac{\partial \zeta}{\partial t} = -\frac{1}{2} v - \frac{1}{2} y\delta \ , \tag{5.1}$$

where ζ is a nondimensional vertical component of relative vorticity, and the dissipation of the relative vorticity is not considered here.

As mentioned in Section 3, the meridional structure of ζ consists mainly of $\zeta_1 D_1$ and $\zeta_3 D_3$. Thus (5.1) can be broken down into two equations, respectively, for ζ_1 and ζ_3,

$$\frac{\partial \zeta_1}{\partial t} = -\frac{1}{2} v_1 - \frac{1}{2}(\delta_0 + \sqrt{2}\,\delta_2) \ , \tag{5.2a}$$

$$\frac{\partial \zeta_3}{\partial t} = -\frac{1}{2}v_3 - \frac{1}{2}(3.24\delta_2) \ , \tag{5.2b}$$

where the relations $yD_0 = D_1$ and $yD_2 = \sqrt{2}D_1 + 3.24D_3$ are used in derivations of (5.2a) and (5.2b).

Since processes controlling propagation for ζ_1 and ζ_3 are similar, we show vorticity analysis only for ζ_1 at day 8. In Exp. K, the maxima of negative (positive) vorticity tendency $\frac{\partial \zeta_1}{\partial t}$ (Fig. 7a), solid line) to the east of 80°E are located to the east of the negative (positive) ζ_1 maxima (Fig. 7a), dashed line), indicating eastward propagation. The vorticity tendency comes mainly from the term $-\frac{1}{2}\delta_0$, suggesting that the eastward propagation is caused by the interaction between Earth's rotation and lower-troposphere convergence (divergence effect). To the west of 80°E the maxima of positive vorticity tendency are located to the west of the positive ζ_1 maxima which means westward propagation. The vorticity tendency here is dominated by term $-\frac{1}{2}v_1$, implying that the westward propagation is caused by the interaction of lower-tropsphere circulation with the meridional gradient of Earth's vorticity (beta effect).

In Exp. R, the positive and negative maxima of the vorticity tendeneies $\frac{\partial \zeta_1}{\partial t}$ are located to the west of the positive and negative maxima of the vorticity ζ_1 (Fig. 7b), which indicates the westward propagation. The terms of $-\frac{1}{2}v_1$ and $-\frac{1}{2}(\sqrt{2}\delta_2)$ have comparable magnitudes. The positive maximum of term $-\frac{1}{2}(\sqrt{2}\delta_2)$ is to the east of the positive maximum of ζ_1 whereas the positive and negative maxima of term $-\frac{1}{2}v_1$ are located to the west of the positive and negative maxima of the vorticity ζ_1. Thus the term $-\frac{1}{2}v_1$ is responsible for the westward propagation. In Fig. 7c, the maximum (minimum) of vorticity tendency is at the north (south) of maximum (minimum) of the vorticity in the Northern (Southern) Hemisphere so that the waves propagate northward (southward). The vorticity tendency is dominated by the interaction of lower-troposphere convergence with Earth's vorticity ($-\frac{1}{2}y\delta$). The westward and poleward propagation of the Rossby waves is similar to the hurricane beta-drift (e.g., Evans et al., 1991; Li and Wang, 1994), but the mechanisms which cause the propagation are different. Since model used here excludes the horizontal advection process, the poleward propagation results from the divergence interaction with Earth's vorticity, which is similar to the cases examined by Holland (1983) in his tropical cyclone motion study.

VI. SUMMARY

In this paper the model developed by Bin Wang, which includes convection-wave convergence feedback and convection-frictional convergence feedback, was used to simulate the behaviors of equatorial waves. Simulation results from two major experiments are analyzed: one initiated with a Kelvin wave (Exp. K) and the other with a Rossby wave (Exp. R).

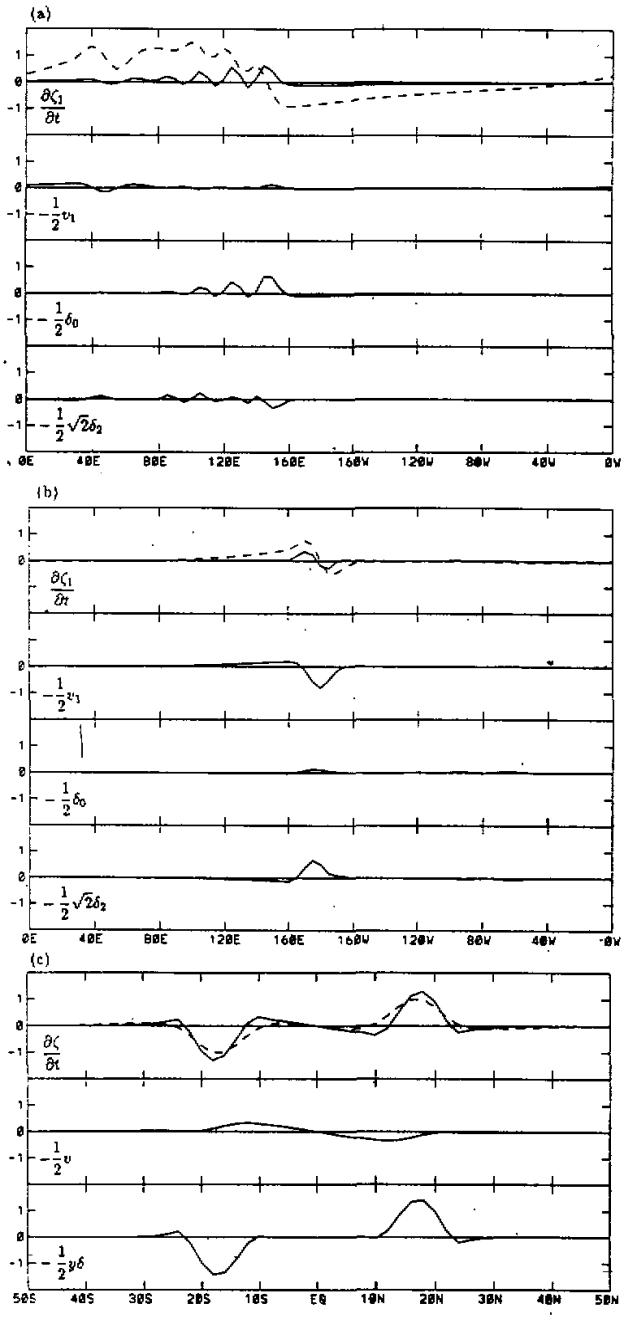

Fig. 7. Longitudinal distributions (solid lines) of terms of Eq. (5.2a) at day 8 in (a) Exp. K and (b) Exp. R, and (c) latitudinal distributions (solid lines) of terms of Eq.(5.1) at day 8 in Exp. R. The dashed lines in (a) and (b) denote ζ_1, the dashed line in (c) represents ζ.

The meridional structures of the equatorial waves are partitioned using Parabolic Cylinder Function (PCF). The equatorial waves in Exp. K have a very large component of Kelvin wave and a minor component of Rossby wave whereas those in Exp. R have a large component of Rossby wave. We define equator mode and off-equator mode as order-0 PCF mode and sum of PCF modes $n \geq 0$ respectively. Thus the equator mode represents the wave structure with a positive precipitation center at the equator whereas the off-equator mode denotes the wave structure with positive precipitation centers off the equator. The main difference of equatorial waves between Exps. K and R is that in Exp. K the equator mode is much stronger than the off-equator mode and vice versa in Exp. R.

The equatorial waves grow much faster in Exp. R than in Exp. K. The energy budgets are calculated to examine the energy source responsible for the development of the equatorial waves. The total energy associated with the equatorial waves is mainly contributed by the eddy available potential energy (EAPE). The EAPE is generated by interactions of lower-troposphere perturbation geopotential with lower-troposphere divergence (convection-wave convergence feedback) and with boundary-layer convergence (convection-frictional convergence feedback). We found that the generation rate of the EAPE by the interaction of lower-troposphere perturbation geopotential with lower-troposphere divergence and the generation rate of the EAPE of the equator mode by interaction of lower-troposphere perturbation geopotential with boundary-layer convergence are about the same for both experiments. The generation rate of the EAPE of the off-equator mode is much larger in Exp. R than in Exp. K causing rapid growth of the equatorial Rossby waves in Exp. R. This is a result of that the lower-troposphere perturbation geopotential of the off-equator mode is much lower in Exp. R than that in Exp. K due to dominant off-equator mode in Exp. R.

The relative vorticity tendency is analyzed to determine the dominant processes responsible for zonal and meridional wave propagation. The vorticity tendency is determined by the interactions between free-atmosphere circulation and the meridional gradient of Earth vorticity (beta effect) and between free-troposphere convergence and Earth vorticity (divergence effect) since nonlinear advection and dissipation are excluded in the present model. The divergence effect is responsible for eastward and poleward wave propagation, whereas the beta effect results in westward wave propagation.

In this study, we show that equatorial Kelvin and Rossby waves may resemble the MJO and twin cyclones along the equator respectively, and both waves can grow under the same uniform sea surface temperature. In reality, MJO may develop sometimes whereas the twin cyclones may grow sometimes. Question is under what condition the equatorial Kelvin or Rossby waves develop. Non-uniform sea surface temperature may be a factor for the preference of the wave development. Another possibility is that development of the equatorial waves may be mechanism dependent. Thus further study is needed to clarify these issues.

We wish to thank Prof. B. Wang for providing us with his model that enabled us to carry out this study. This research is supported by Canadian National Science and Engineering Research Council and Atmospheric Environment Service research grants.

REFERENCES

Chang, C. -P., and H. Lim (1988), Kelvin wave-CISK: A possible mechanism for the 30-50 day oscillation, *J. Atmos. Sci.*, **45**: 1709-1720.

Emanuel, K. A. (1987), An air-sea interaction model of intraseasonal oscillation in the tropics, *J. Atmos. Sci.*,

44: 2324–2340.

Evans, J. L., G. J. Holland, and R. L. Elsberry (1991), Interactions between a barotropic vortex and an idealized subtropical ridge, Part I: Vortex motion, *J. Atmos. Sci.*, **48:** 301–314.

Hayashi, Y. (1970), A theory of large-scale equatorial waves generated by condensation heat and accelerating the zonal wind, *J. Meteor. Soc. Japan*, **48:** 140–160.

Gill, A. E. (1980), Some simple solutions for heat-induced tropical circulation, *Quart. J. R. Met. Soc.*, **106:** 447–462.

Holland, G. J. (1983), Tropical cyclone motion: Environmental interaction plus a beta effect, *J. Atmos. Sci.*, **40:** 328–342.

Kuma, Ken-ichi (1994), The Madden and Julian oscillation and tropical disturbances in an aqua-planet version of JMA global model with T63 and T159 resolution, *J. Meteor. Soc. Japan*, **72:** 147–172.

Lau, K. -M., and L. Peng (1987), Origin of Low-frequency (intraseasonal) oscillations in the tropical atmosphere, Part I: Basic theory, *J. Atmos. Sci.*, **44:** 950–972.

Li, X, and B. Wang (1994), Barotropic dynamics of the beta gyres and beta drift, *J. Atmos. Sci.*, **51:** 746–756.

Lindzen, R. S. (1974), Wave-CISK in the tropics, *J. Atmos. Sci.*, **31:** 156–179.

Madden, R. A., and P. R. Julian (1971), Description of a 40–50 day oscillation in the zonal wind in the tropical Pacific, *J. Atmos. Sci.*, **28:** 702–708.

Madden, R. A., and P. R. Julian (1972), Description of global-scale circulation cells in the tropics with a 40–50 day period, *J. Atmos. Sci.*, **29:** 1109–1123.

Neelin, J. D., I. M. Held, and H. Cook (1987), Evaporation-wind feedback and low-frequency variability in the tropical atmosphere, *J. Atmos. Sci.*, **44:** 2341–2348.

Wang, B. (1988), Dynamics of tropical low-frequence waves: An analysis of the moist Kelvin waves, *J. Atmos. Sci.*, **45:** 2051–2065.

Wang, B., and T. Li (1993), A simple tropical atmosphere model of relevance to short-term climate variations, *J. Atmos. Sci.*, **50:** 260–284.

Wang, B., and T. Li (1994), Convective interaction with boundary-layer dynamics in the development of a tropical intraseasonal system, *J. Atmos. Sci.*, **51:** 1386–1400.